Kinetic Pathway of Pattern-Directed Phase Separation in Binary Polymer Mixture Films

Li-Tang Yan,*,† Jialin Li, Yao Li, and Xu-Ming Xie*

Advanced Materials Laboratory, Department of Chemical Engineering, Tsinghua University, Beijing 100084, P. R. China

Received November 25, 2007; Revised Manuscript Received February 13, 2008

ABSTRACT: The phase separation of polymer blend films on the stripe patterned surface is numerically investigated by coupling the Flory–Huggins−de Gennes equation with the Cahn−Hilliard−Cook equation. The kinetic pathway and its mechanisms are analyzed in both real space and reciprocal space. Compared to experimental measurements, the simulated results exhibit more complete kinetic pathways of pattern-directed phase separation. It is found that the extreme fluctuation of the chemical potential at the edges of stripes leads to the formation of the branch structure. Our simulated results indicate that the phase inversion, occurring not only in the polymer/air interface but also in the bulk, can extensively affect the relations between the isotropic phase separation and the periodic structure. The analysis in reciprocal space shows that the evolution of the phase morphologies in the polymer/air interface obeys a $^1/_3$ power law for a thick film, consistent with the experimental results. It is also found that the amplitude change of the first diffraction peak can reflect the kinetic pathway of the phase structure in the polymer/air interface very well. A narrower strip periodicity corresponds to an earlier phase inversion and an earlier appearance of the droplet arrays in strips.

1. Introduction

The effect of surface on the phase separation behavior of polymer mixtures has recently attracted considerable interest both theoretically[1] and experimentally.[2–4] Differences between the wetting properties of coexisting phases at the respective boundaries will influence the kinetics of separation as well as the resulting equilibrium domain structures in the film, leading to surface-directed phase separation. Patterning the surface such that there are ordered patches with different surface interactions has been a recent extension to previous surface work.[5–8] It is possible to create organized structure in ultrathin polymer blend films by chemically modulating the substrate to guide their organization into regular patterns. Laterally ordered domain structures[5,8] of different periodicity have been successfully created via surface-directed phase separation on substrate with suitably chosen surface energy, i.e., a patterned surface. These techniques exploit the sensitivity of the phase-separating blends to symmetry-breaking perturbations to guide phase separation, and they can also be defined as pattern-directed phase separation (PDPS).[6] The PDPS of the polymer system, which could promote the understanding of phase equilibria near surfaces on a molecular level and might provide a simple means for fabricating polymer-bases microelectronic circuits or polymer resists for lithographic semiconductor processing, is of great theoretical and technological importance.

A variety of experimental methods have been applied to blend films on patterned surfaces.[5–11] These experimental works mainly focus on the relations between the polymer morphologies and the patterned surface, the factor limiting the control of surface structure in polymer films and the tuning approach of surface pattering in thin polymer blend films at a smaller scale. For example, Nisato et al.[6] also considered the phase separation kinetics of ultrathin polymer blend films spun cast onto striped substrates in the real space and its reciprocal space. They observed a coupling between phase separation and the surface modes in which the phase separation process excites surfaces modes of a commensurate scale. Almost all experiments also showed that the perfectness of the order phase structure varies with the pattern as well as with film thickness. Along with the experimental measurement, computer simulation is playing an increasingly important role in understanding the mechanism of morphologies changes in PDPS.[12,13] For instance, employing the traditional Cahn−Hilliard−Cook (CHC) model augmented by a surface energy term, Muthukumar and co-workers[13] first investigated phase separation of a binary blend near a patterned surface in three dimensions (3D). They studied the phase morphologies with different thicknesses and periodicities of the surface, and examined the effect of noise on the morphologies. They also observed the checkerboard-like transient states as in the case of two-dimensional (2D) simulations.[12a]

Although both theoretical and experimental works have exploited PDPS to a certain extent, yet the question as to the factors limiting the control of surface structure in polymer films is still an open one, and the ultimate goal of nanofabrication has remained elusive even up to now. It is clear that progress in this field requires a better understanding of the detailed and complete kinetics and its mechanisms governing surface pattern formation in thin polymer film, which is also the issue we would like to study in this work by the numerical technique.

In this paper, we numerically investigate the PDPS with stripe patterned surfaces in 3D space by coupling the CHC model with the Flory–Huggins−de Gennes (FHdG) model, which better fits the polymer blend. Compared to the corresponding experimental observations, the phase morphologies and its evolution of polymer films near patterned surfaces are considered in both real space and reciprocal space. Our main purposes are to exhibit a more complete and detailed kinetic pathways of PDPS in binary polymer mixture and to gain insight into the kinetic mechanisms.

2. Model and Numerical Procedure

The dynamics and morphologies evolution are described by the CHC equation for diffusive field with binary mixtures (A and B), which can be written as[14]

* Corresponding authors. Email: li-tang.yan@uni-bayreuth.de (L.-T.Y.); xxm-dce@mail.tsinghua.edu.cn (X.-M.X.).

† Current Address: Department of Physical Chemistry II, Universität Bayreuth, D-95440 Bayreuth, Germany.

10.1021/ma702616s CCC: $40.75 © 2008 American Chemical Society
Published on Web 04/25/2008

$$\frac{\partial \phi}{\partial t} = M\nabla^2 \frac{\delta F\{\phi(r,t)\}}{\delta \phi(r,t)} + \eta(r,t) \quad (1)$$

Here $\phi(r, t)$ is the local fraction of component A at point r at time t. M is a phenomenological parameter characterizing the self-diffusion ability. $\eta(r, t)$ is the thermal noise. The same degree of polymerization, $N_A = N_B = N$, is set for a symmetric binary system. Hydrodynamic effect is neglected throughout, as although it may play an important role in the very late stage of phase separation, the early and intermediate stages should not be affected. In order to study phase separation in polymer mixture, for F, the FHdG free energy (in units of k_BT) is chosen and is given by eq 2, where χ is the temperature-dependent Flory–Huggins dimensionless interaction parameter and b is the Kuhn statistical segment length.[15] The integral is performed over the volume, V, of the sample.

$$F(\phi) = \int_V \mathrm{d}r \left[\frac{\phi}{N}\ln(\phi) + \frac{(1-\phi)}{N}\ln(1-\phi) + \chi\phi(1-\phi) + \frac{b^2}{36\phi(1-\phi)}|\nabla\phi|^2\right] \quad (2)$$

In terms of the deduction of Puri,[16] the boundary conditions of surface-directed phase separation dynamic model based on CHC equation can be described by two partial differential equations. The first equation is defined as eq 3, where h_1, g, and γ are three parameters characterizing the static surface diagram.[16] h_1 characterizes the surface potential which models the preferences of the surface for one of the components. g characterizes the exchange interaction between sites on the surface in the underlying microscopic model. γ is the parameter which has a relation with the bulk correlation length. z_0 is the location of the surface. A second boundary condition, $\Delta J|_{z=z_0} = 0$, where J, defined as $J = \nabla\delta F|\delta\phi$, is the polymer flux, and it is used to ensure that the flux of polymer components through the surface boundary is zero, which enforces conservation of the order parameter. In the present study, we choose the z axis as the direction of the surface effect and consider only one surface located at the $x-y$ plane with $z_0 = 1$

$$\frac{\partial \varphi(x, z_0, \tau)}{\partial_\tau} = -h_1 - g\varphi(x, z_0, \tau) + \gamma \left.\frac{\partial \varphi(x, z, \tau)}{\partial z}\right|_{z=z_0} \quad (3)$$

It has been proved that the calculated results are more precise if eq 3 is coupled into the dynamic model.[17] Thus, by lumping together eqs 1−3, and by rescaling into a dimensionless form, the dynamic equation can be obtained as follows in eq 4. χ_s is the spinodal value of χ at $\phi = \phi_0$, i.e., $\chi_s = 1/[2N\phi_0(1-\phi_0)]$, where ϕ_0 is the initial average concentration of component A, with $\phi_0 = 0.5$ for the critical condition in the present simulations. χ_c is the value of χ at the critical point and $\chi_c = 0.01$ in this study. χ_f is the deepest quench. $\bar{r}$ and τ are rescaled spatial and temporal variables respectively, given by $\bar{r} = (|\chi_f - \chi_s|)^{1/2} r/b$, and $\tau = NM(\chi_f - \chi_s)^2 t/b^2$ is the Dirac-delta function, ensuring that the surface free energy only affects $z_0 = 1$.

$$\frac{\partial \phi(\bar{r}, \tau)}{\partial \tau} = \frac{1}{2}\nabla^2\left[\frac{\chi_c}{2(\chi_f - \chi_s)}\ln\frac{\phi}{1-\phi} - \frac{2\chi}{\chi_f - \chi_s}\phi + \frac{2\phi - 1}{36\phi^2(1-\phi)^2}(\nabla\phi)^2 - \frac{1}{18\phi(1-\phi)}\nabla^2\phi + \left(-h_1 - gg\varphi + \gamma\left.\frac{\partial\varphi}{\partial z}\right|_{z=z_0}\right)\delta(z)\right] \quad (4)$$

In essence, the surface potential used in the model is short-range because the power law potential, depending on the distance from the surface, is not included in it.[16] It should be noted that the temperature dependence of the mobility is not explicitly considered because the time steps are scaled by the mobility. Hence, the difference between mobility for different quench depths can be reflected in a different scaling factor from numerical time to real time. Importantly, the structural growth is not affected by this assumption.[17] Equation 4 can be solved using the finite difference approach.[18] Numerically, for the sake of numerical stability and higher accuracy, the Laplacian ∇^2 is discretized based on the cell dynamics scheme (CDS) proposed by Oono and Puri.[19] It is then transformed as[20]

$$\nabla^2 X \rightarrow \frac{1}{\xi^2}(\langle\langle X\rangle\rangle - X) \quad (5)$$

where ξ is the cell size. $\langle\langle X(\bar{r},\tau)\rangle\rangle$ represents the following summation of $X(\bar{r})$ for the nearest neighbors ($\bar{r}$) and the next-nearest neighbors, ($\bar{r}$,$\bar{r}$)and the next-next-nearest neighbors ($\bar{r}$,$\bar{r}$,$\bar{r}$):

$$\langle\langle X(\bar{r})\rangle\rangle = B_1\sum_{\bar{r}=\bar{r}.} X(\bar{r}) + B_2\sum_{\bar{r}=\bar{r}.\bar{r}.} X(\bar{r}) + B_3\sum_{\bar{r}=\bar{r}.\bar{r}.\bar{r}.} X(\bar{r}) \quad (6)$$

where, B_1 B_2, and B_3 are 6/80, 3/80, and 1/80 for the 3D system. In order to avoid the discretization effect due to the lattice size,[17] the surface terms h_1, g, and γ are rescaled by the step length of the spatial discretization, $\Delta\bar{r}$, and are listed as follows:

$$h_1 \rightarrow h_1/\Delta\bar{r}, \quad g \rightarrow g/\Delta\bar{r}, \quad \gamma \rightarrow \gamma/\Delta\bar{r} \quad (7)$$

Our simulations are carried out on a 3D lattice with size 256 × 256 in the $x-y$ plane. Free boundary conditions are applied at the other end in the z direction. Thus, the interactions of polymers A and B with respect to air are omitted for the free fluctuation in the polymer/air interface. The periodic boundary conditions are applied in x and y directions. Noise, with a magnitude of $\pm 1 \times 10^{-3}$, is only added once at the start of the quench. In our simulations, the spatial discretization step, $\Delta\bar{r}$, is chosen such that the characteristic length for the early stage spinodal decomposition, l_{sp}, is equal to 8. The periodicity of the stripe patterned surface is denoted by λ. Various values of λ ($\lambda = l_{sp}$, $2l_{sp}$, $4l_{sp}$, $6l_{sp}$, and $8l_{sp}$) are selected to examine the effect of the stripe periodicity. The interaction strengths of the surface potential, h_1 are alternately set 0.05 and −0.05 for the neighboring strips except for the special explanation. $g = 0.1$, $\gamma = 0.1$, and $N = 200$ are set in all simulations. To simplify the numerical procedure, and to avoid having to rescale the lattice, $\chi_f - \chi_s$ is chosen to be the same before and after the quench, and it is fixed at 0.0133 throughout simulations. A dimensionless parameter, ε, which is defined as $\varepsilon = (\chi - \chi_c)/\chi_c$, denotes the quench depth in this work, and $\varepsilon = 0.1$ is set for all simulations except for the special explanation. The Δt (time step) value used during the temporal discretization was 1×10^{-4}.

3. Results and Discussions

In this section, the phase structure and its evolution kinetics are first analyzed on the basis of simulated images in real space. To extensively exploit the relations between the isotropic phase separation and the periodic structure, these images are then transformed into reciprocal space by 2D Fourier Transformation (2DFT).

3.1. Phase Morphologies and Evolution Kinetics. We would first like to show the formation and evolution of phase morphologies in 3D space. The 3D patterns illustrating the development of phase morphologies with film thickness $l = 2l_{sp}$ and strip periodicity $\lambda = 4l_{sp}$ are listed in Figure 1. The concentration of component A is marked with the color bar. There are two interfaces, i.e., surface/polymer and polymer/air, in the PDPS system. In the simulations throughout the paper, the surface/polymer interface is set in the $x-y$ plane with $z =$

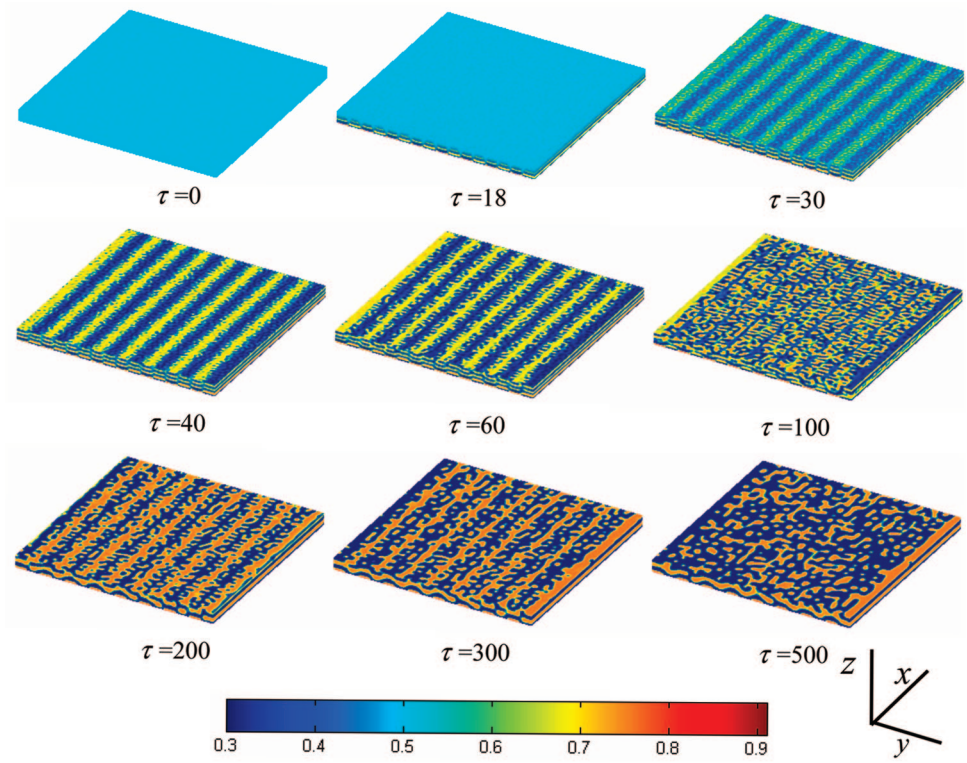

Figure 1. 3D patterns showing the development of the polymer morphologies following $l = 2l_{sp}$ and $\lambda=4l_{sp}$. The color bar indicates the concentration of the wetting component for the substrate.

1 and the polymer/air interface locates at the $x-y$ plane with $z = 2\ l_{sp}$. It can be seen that the fluctuation wave induced by the stripe pattern penetrates into the bulk gradually. In the lateral side, a checkerboard-like structure comes into being. However, with the increasing time, the structure coarsens, which reproduces the results in previous simulated works.[12a,13]

Some general characterization methods, e.g., AFM, SEM, et al., really examine the kinetic pathway in polymer/air interface. As shown in Figure 1, no phase-separated structure can be discerned in the polymer/air interface at the initial time. With the increasing time, the stripe structure occurs in this interface and becomes clear, and the phase structure exhibits the typical in-phase state where the component in each strip corresponds to the chemical potential in the patterned surface. Some branch structures then form at the edges of strips. These branches grow up and the original in-phase order structures break up gradually. However, the branches can enrich again in the next strip in this interface. At about $\tau = 200$, a clear out-of-phase pattern, where the component in each strip does not correspond to the surface pattern, is visible in the polymer/air interface. Clearly, a phase inversion at the stripes occurs during this stage and in this interface. The edges of these new stripes can be destroyed as the images after $\tau = 200$, and the stripes tend to break up again. Finally, the stripe pattern in the polymer/ air interface are replaced by arrays of fairly uniformly spaced droplets, corresponding to the experimental observations of Nisato et al.[6] Our simulated results also numerically indicate that the formation of the droplet arrays may be a universal phenomenon and is only a part of a complete kinetics of PDPS.

Figure 2 illustrates the time series of phase morphologies with the same conditions except the stripe periodicity of the patterned surfaces. From left to right, the periodicity becomes narrower. It can be found that phase inversion always occurs for every periodicity, when the branch structures form at the edges of strips. For the narrower periodicities with $\lambda = 2l_{sp}$ and l_{sp}, the branches can connect with each other as some bridges between two close stripes with the same surface chemical potential, forming the interconnecting net morphologies which has been observed in experiments.[9] Regardless of periodicity, all stripe patterns will undergo phase inversion and finally break up into droplet arrays along the stripes. Moreover, one can note that a narrower periodicity corresponds to an earlier appearance of the droplet arrays, which demonstrates that the system with a bigger periodicity is easy to form a steadier order film structure.

To analyze the phase morphologies of PDPS system in more detail, the structures inside the blend films are also investigated. Figure 3 is an example showing the phase morphologies in $y-z$ planes at varying x axis (Figure 3a) and those in $x-z$ planes at varying y axis (Figure 3b). It can be seen from Figure 3a that, in $y-z$ planes, the composition waves penetrate into the bulk and the strips with different surface potentials can induce alternate fluctuation for two components along z axis, leading to the checkerboard-like structure. In Figure 3b, $y-z$ planes at the strips with $h_1 = 0.05$ ($x = 24$) and $h_1 = -0.05$ ($x = 72$) and at the borders of two neighboring stripes ($x = 128$, 176, and 224) are selected, respectively. Clearly, alternate component fluctuation along the z axis occurs in the $y-z$ planes at the stripes. However, the $y-z$ planes at the borders of two neighboring stripes, especially in the bulk, undergo phase separation like the spinodal decomposition, demonstrating a more extreme component fluctuation at the border of two neighboring strips.

3.2. Formation Mechanism of the Phase Inversion. In order to analyze the kinetic process in detail, here we introduce a parameter, $p(z,\tau)$, which can be defined as follows:[21]

$$P(z,\tau) = \sum_{x,y} \frac{\phi(x,y,z,\tau)\sigma(x,y)}{L^2|\phi(x,y,z,\tau)|} \tag{8}$$

Here L is the side size of the $x-y$ plane. $\sigma(x,y)$ describes the preassigned pattern on the surface, and $\sigma(x,y) = 1, -1$, respectively, denotes the A, B preferring element of the surface. If the domain morphologies at a plane z and at time τ is perfectly in-phase, $P(z,\tau) = 1$, while $P(z,\tau) = -1$ if the morphologies is

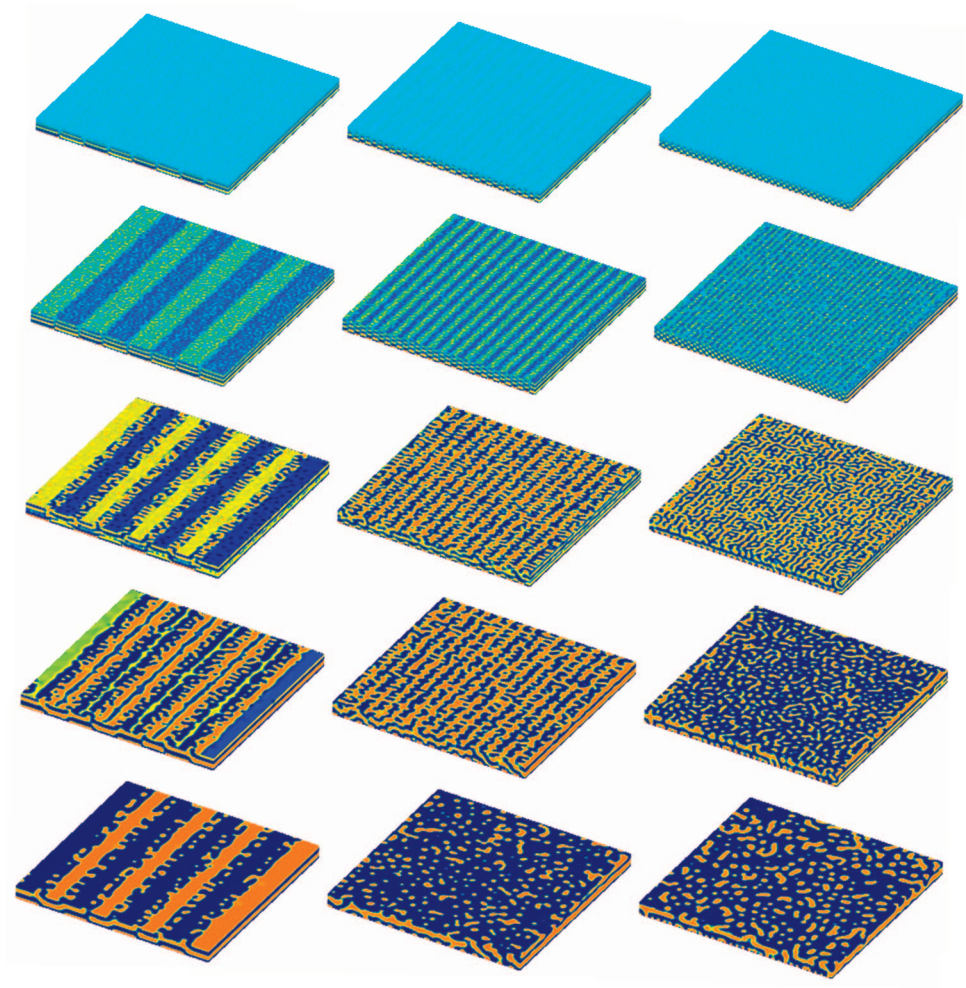

Figure 2. Development of the polymer morphologies following $l = 2l_{sp}$ and different periodicities. From left to right: $\lambda = 8l_{sp}$, $2l_{sp}$, l_{sp}. From top to bottom: $\lambda = 20$, 30, 100, 200, 500. The color bar and the coordination are the same as those of Figure 1.

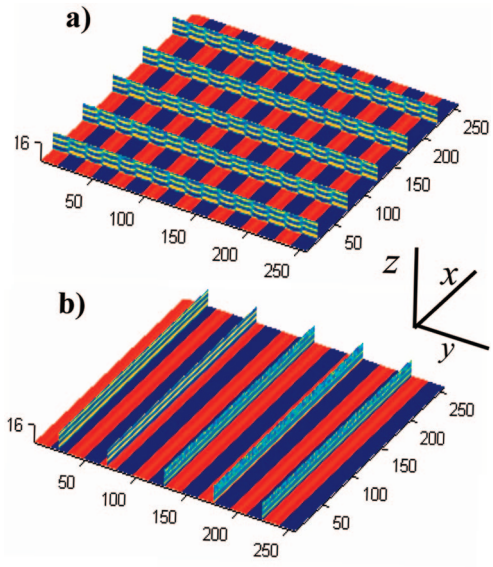

Figure 3. Phase morphologies in different planes with $l = 2l_{sp}$, $\lambda = 4l_{sp}$, and $\tau = 30$. The color bar is the same as those of Figure 1: (a) $y-z$ planes along x axis, $x = 20$, 70, 120, 170, and 220; (b) $x-z$ planes along y axis, $y = 24$, 72, 128, 176, and 224. The $x-y$ planes in both parts a and b locate at $z = 1$.

totally out-of-phase. Any intermediate value of $P(z,\tau)(-1 < P(z,\tau) < 1)$ would correspond to a domain morphologies between these two extremes.

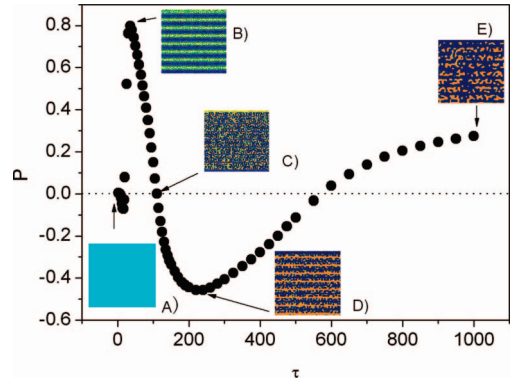

Figure 4. Time evolution of $P(z,\tau)$, in the polymer/air interface with $l = 2l_{sp}$ and $\lambda = 4l_{sp}$. The color bar is the same as those of Figure 1. In the inset, the morphologies at different times are exhibited. Key: (A) $\tau = 0$; (B) $\tau = 30$; (C) $\tau = 110$; (D) $\tau = 220$; (E) $\tau = 1000$.

Figure 4 illustrates the temporal evolution of $P(z,\tau)$ in the polymer/air interface. The inset exhibits snapshots at different times. One can found that $P(z,\tau) \approx 0$ at start because the fluctuation wave induced by the patterned surface does not reach the interface. With the increasing time, $P(z,\tau)$ increases, and it reaches a maximum at about $\tau = 30$, where the phase approximates to perfectly in-phase. Then, $P(z,\tau)$ decreases while the stripes break up due to the formation of branch structure in this interface. At about $\tau = 220$, $P(z,\tau)$ approximates to a minimum, corresponding to an out-of-phase structure. $P(z,\tau)$

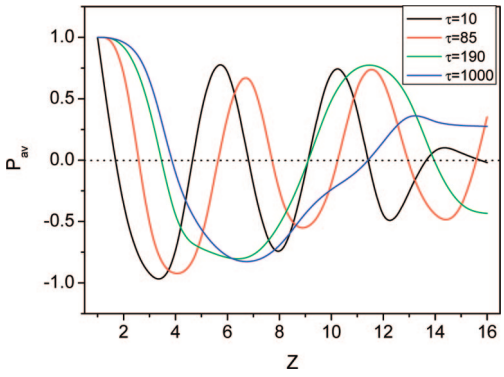

Figure 5. Averaged $P(z,\tau)$ profiles in z direction at different times with $l = 2l_{sp}$ and $\lambda = 4l_{sp}$.

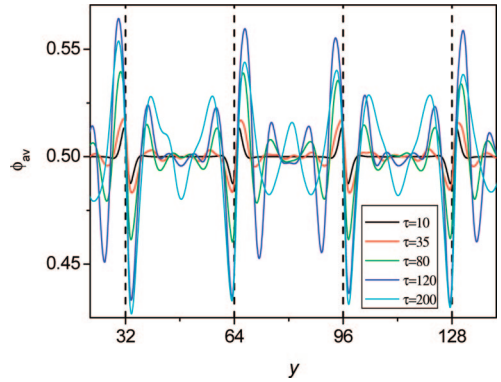

Figure 6. Lateral concentration profiles along the y axis, where $l = 2l_{sp}$ and $\lambda = 8l_{sp}$.

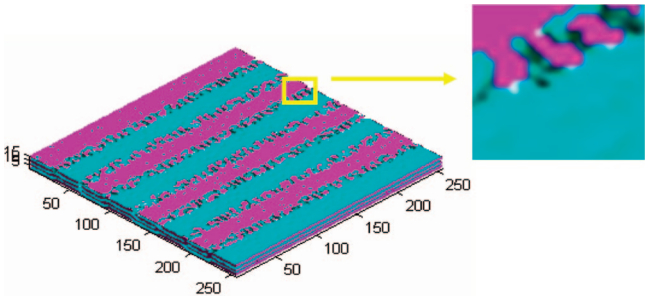

Figure 7. Isophase 3D image showing the complete branch structure with $l = 2l_{sp}$, $\lambda = 8l_{sp}$, and $\tau = 35$.

keeps fluctuating; however, the scope becomes weaker because the droplet array comes into being at the final stage.

To verify the degree of phase inversion in different parallel planes along z axis, the averaged $P(z,\tau)$ profiles are also obtained by averaging $P(z,\tau)$ in the $x-y$ planes with different z for a single run and then ensemble averaging over 10 different runs. The averaged $P(z,\tau)$ profiles in the z direction, corresponding to Figure 1, at different times are shown in Figure 5. One can note that $P_{av}(z,\tau)$ approximates to 1 near the surface. However, it oscillates in the bulk, demonstrating the alternation of the in-phase and out-of-phase along z direction as shown in Figure 3. Moreover, with the increasing time, the profile slowly propagates out into the bulk, just as the lateral averaged concentration profile.[16]

The average concentration profile along y axis with $l = 2l_{sp}$ and $\lambda = 8l_{sp}$ is calculated as eq 9

$$\phi_{av}(y,\tau) = \frac{1}{N_{x,z}} \sum_{x,z} \phi(x,y,z,\tau) \tag{9}$$

where $N_{x,z}$ is the total mesh points in one $x-z$ plane. Figure 6 illustrates these profiles at different times. Clearly, the extreme concentration fluctuation happens at each boundary of two stripes with different chemical potentials. An isophase 3D image, where component B has been erased, as in Figure 7, shows the complete structure of these branches. It can be seen that each branch connects with the same component in the close stripe. Thus, both Figure 6 and Figure 7 demonstrate that the branches are really the channels where the same component flows between two close stripes.

What drives the flow of the same component between two close stripes? For the sake of answering this question, the chemical potential, $\mu(x,y,z)$, is considered and can be calculated as follows:

$$\mu = \frac{1}{N(\chi_f - \chi_s)} \ln\frac{\phi}{1-\phi} - \frac{2\chi}{\chi_f - \chi_s}\phi + \frac{2\phi - 1}{36\phi^2(1-\phi)^2}(\nabla\phi)^2 - \frac{1}{18\phi(1-\phi)}\nabla^2\phi + \left(-h_1 - g\phi + \gamma\frac{\partial\phi}{\partial z}\Big|_{z=z_0}\right)\delta(z) \tag{10}$$

Then, the lateral average chemical potential, μ_{av}, along the y axis can be calculated as eq 11.

$$\mu_{av}(y,\tau) = \frac{1}{N_{x,z}} \sum_{x,z} \mu(x,y,z,\tau) \tag{11}$$

where $N_{x,z}$ is also the total mesh points in one $x-z$ plane. The fluctuation degree of the chemical potential can be used to characterize the activity of the blends, and a stronger fluctuation of the chemical potential indicates a higher possibility for the occurrence of phase separation.[1,22] Figure 8 is the plot of μ_{av} against y. It can be seen that more extreme fluctuation of the chemical potential occurs at the edges of stripes. Thus, phase separation tends to appear at the edges of stripes, leading to the formation of the branch structure. With the time increasing, components A and B will penetrate from one strip to its neighboring strips each other through the branch structure. The phase gradually inverses at strips.

To gain insight into the formation mechanism of the phase inversion between neighboring stripes, the phase morphologies with different quench depths (ε) and different surface potentials (h_1) are illustrated in Figure 9. Compared to the conditions of Figure 1, only the quench depth is changed from $\varepsilon = 0.1$ to $\varepsilon = 0.04$ for Figure 9a,b and only the alternate surface potentials of the strips are changed from $h_1 = \pm 0.05$ to $h_1 = \pm 0.1$ for Figure 9c,d. Clearly, the phase morphologies in this figure at the same times have great changes compared to those in Figure

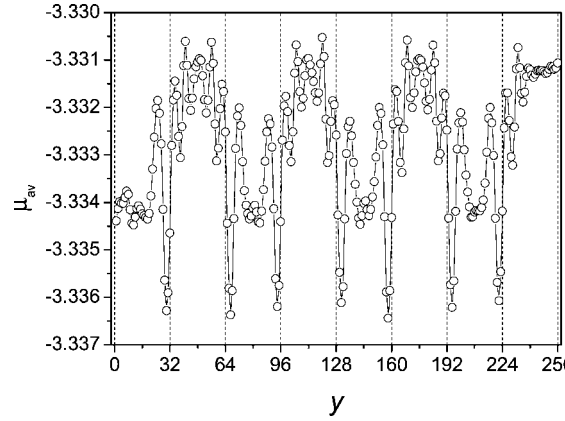

Figure 8. Plot of chemical potential against y with $l = 2l_{sp}$, $\lambda = 8l_{sp}$, and $\tau = 35$.

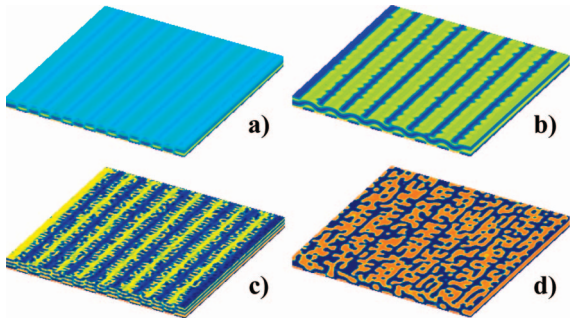

Figure 9. 3D patterns showing the polymer morphologies with different conditions following $l = 2l_{sp}$ and $\lambda = 4l_{sp}$. The color bar and the coordination are the same as those of Figure 1. Key: (a) $\varepsilon = 0.04$, $\tau = 40$; (b) $\varepsilon = 0.04$, $\tau = 500$; 9c) $h_1 = \pm 0.1$, $\tau = 40$; (d) $h_1 = \pm 0.1$, $\tau = 500$.

1. It can be found that a deeper quench depth is prone to restrain the phase inversion and to hold the regular phase structure in the polymer\air interface. A higher surface potential in the strips can lead to an earlier and faster phase inversion. Thus, these tow factors can be used to tune the phase morphology of PDPS in the experiment. The change of quench depth really corresponds to that of bulk chemical potential.[1] So, combining Figures 8 and 9, one can find that the phase inversion in PDPS system is essentially due to the interplay between the surface potential and the bulk chemical potential.

3.3. Analysis of Kinetic Pathway in Reciprocal Space. The analysis in reciprocal space focuses on the 2DFT of the real space images in the polymer/air interface. As shown in Figure 10a, 2DFT image are characterized by two features:[6,9] a diffusive ring and a series of sharp peaks uniformly distributed along the vertical axis. Radical average of the diffusive ring, which characterizing the isotropic morphologies, is used to determine the spectrums of isotropic component, i.e., $S_i(k)$ (Figure 10b).The squared 2DFT amplitudes forming a narrow (four pixels wide) stripe along the sharp peaks, with $k_n = nk_\lambda$ (n is an integer; $k_\lambda = 1/\lambda$), are averaged to yield the spectrum $S(k)$. The isotropic contribution, $S_i(k)$, is removed from $S(k)$ to yield the spectrum $S_a(k)$ of the anisotropic component (Figure 10c).

The wave-vector magnitude for which the intensity of $S_i(k)$ is a maximum, i.e., the character scattering vector, is denoted as k^*. The systematic k^* for the different samples can be determined through Lorentz line fit as follows:[6]

$$S(k) = a + b/[(k - k^*)^2 + c] \tag{12}$$

where a, b, and c are fitting parameters. Figure 11 plots the temporal evolution of k^* for different periodicities in the polymer\air interface. At the initial stage, k^* exhibits a large scope of fluctuation due to the phase inversion (see Figure 1). However, the fluctuation seems very weak at the intermediate and late stages. The solid line in the figure clarifies that the evolution of the phase morphologies at the stages obeys a $^1/_3$ power law, reproducing the experimental results of Nisato et al.[6] The $^1/_3$ scaling, which characterizes spinodal decomposition, Ostwald ripening, or diffusive coalescence, is commonly found in the early stages of film phase separation in bulk.[22] Besides the effect of the surface potential, the kinetic pathway of PDPS is also affected by the bulk chemical potential. For a thick film, as in the present study or the experiment of Nisato et al., the bulk chemical potential may dominate the phase separation in the stripes. However, for a very thin film, the kinetic mechanism may exhibit diffusion growth law[23] or logarithmic growth law,[24] where the surface potential is a majority effect factor.

Figure 12 illustrates the temporal evolution of the harmonic amplitudes for four diffraction peaks, i.e., J_n ($n = 1, 2, 3, 4$) in the polymer\air interface. According to previous experimental

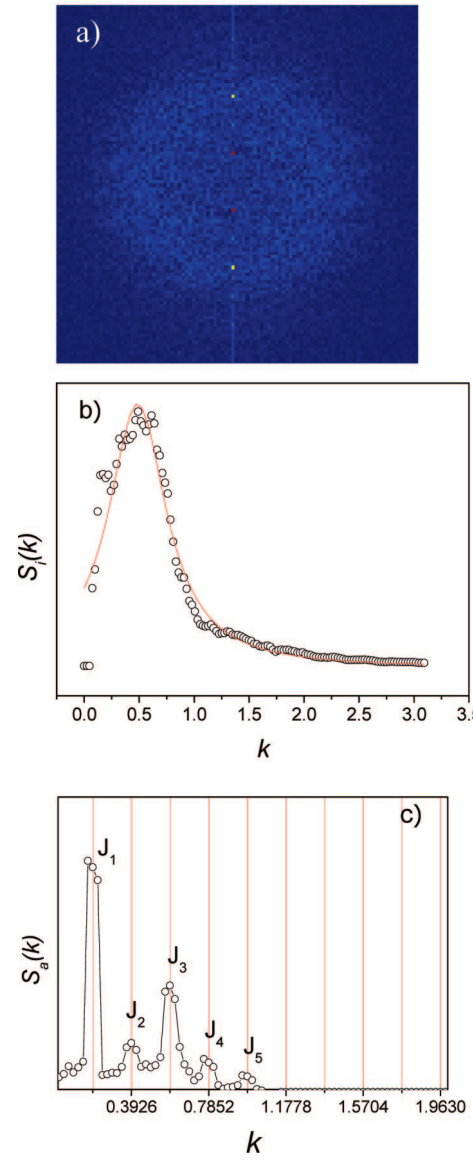

Figure 10. 2D FFT images (a) and the spectra of isotropic component (b) and anisotropic component (c). Here $l = 2l_{sp}$, $\lambda = 4l_{sp}$, and $\tau = 180$. J_n ($n = 1, 2, 3, 4, 5$) denotes the intensity of each peak in the anisotropic spectrum.

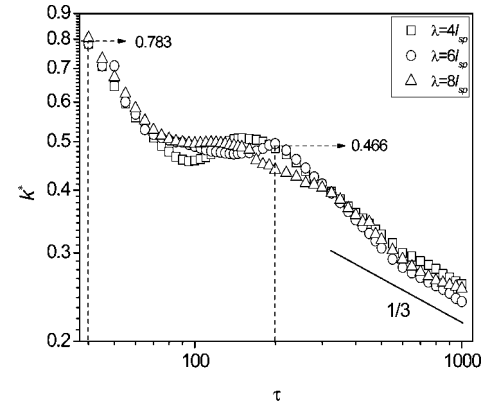

Figure 11. Position of k^*, determined from Lorentz fits to the data, as a function of time in the log–log plot, where $l = 2l_{sp}$.

results of Nisato et al.,[6] the diffraction peak can be excited by the phase separation process when the scale of phase separation becomes commensurate with the period of the striped surface. A diffraction peak in higher frequency becomes excited at an

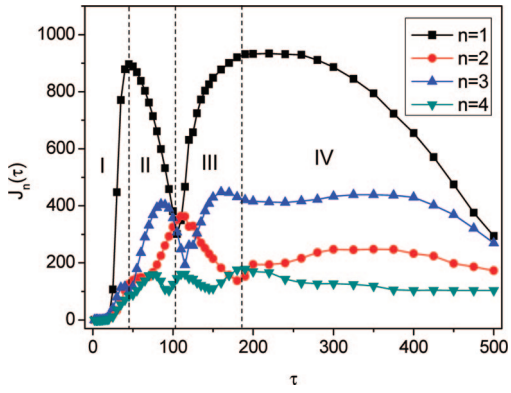

Figure 12. Time evolution of the harmonic amplitudes J_n following $l = 2l_{sp}$ and $\lambda = 4l_{sp}$.

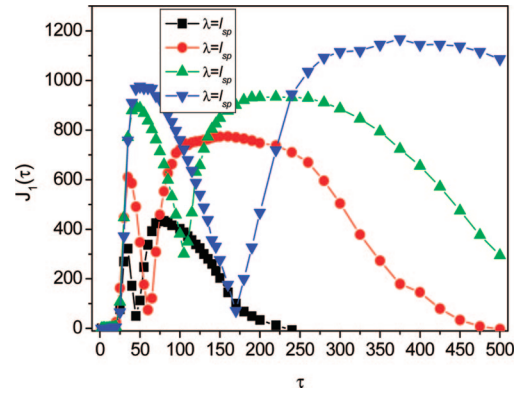

Figure 13. Time evolution of the harmonic amplitudes $J_1(\tau)$with different strip periodicities following $l = 2l_{sp}$.

earlier stage of the phase separation, and these excitations decay with times as the phase separation pattern further coarsens. However, our simulation as shown in Figure 12 demonstrates that the temporal evolution of the harmonic amplitudes fluctuates obviously. After a careful analysis, one can find that these plots can be divided into four regions:

(A) Region I ($\tau \leq 40$).The left arrow in Figure 11 denotes that k^* arrives at about 0.78 at $\tau = 40$. Notice that the location of the fourth diffraction peak is in the $k_4 = 4(2\pi/\lambda) \approx 0.78$ region. Thus, all diffraction peaks are not excited until $\tau = 40$. So, these four diffraction peaks only increase in this region, consistent with the experimental conclusion. As shown in Figure 1, the stripe structure gradually becomes clear in the polymer\air interface during this stage and does not undergo any phase inversion.

(B) Region II ($40 < \tau \leq 110$). Although k^* has passed through 0.78, the fourth diffraction peak does not decay in sequence. However, the first one decays extremely. These variations obviously depart from the experimental conclusion. It should be emphasized that, as shown in Figure 1, some branch structures form at the edges of strips at about $\tau = 40$ in the polymer/air interface. These branches grow up, and the original in-phase order structures are almost destroyed at about $\tau = 110$. At the same time, the amplitude of the first diffraction peak in Figure 12 reaches the minimum.

(C) Region III ($110 < \tau \leq 200$). It can be seen from Figure 11 that k^* arrives at about 0.47 at $\tau = 110$, demonstrating that the character scale of the phase separation locates between the second peak ($k_2 \approx 0.39$) and the third one ($k_3 \approx 0.59$). However, Figure 12 indicates that, in this region, the first peak increases while other peaks decrease. From Figure.1, one can note that the branch structure in the polymer\air interface enriches again in the neighboring strips gradually. At about $\tau = 200$, a clear out-of-phase pattern, where the component in each strip does not corresponds to the surface pattern, is visible in the polymer/air interface. Clearly, the phase inversion at the stripes in this interface finishes at the end of this region. At the same time, the amplitude of the first diffraction peak in Figure 12 reaches at the second maximum gradually.

(D) Region IV ($\tau \geq 200$). After $\tau = 200$, the edges of these new stripes tend to break up again. Finally, the strips in the polymer/air interface are replaced by arrays of fairly uniformly spaced droplets. The amplitude of the first diffraction peak in Figure 12 gradually decreases again.

The above analysis indicates that the phase inversion can extensively affect the relation between the diffraction peaks and the character scale of the phase separation. Thus, the corresponding experimental conclusion drawn by Nisato et al.[6] may be only applied to a phase-separated system without phase inversion. It can also be found that the amplitude change of the first diffraction peak can reflect the kinetic pathway of the phase structure in the polymer\air interface very well. Figure 13 illustrates the temporal evolution of the amplitudes in the first diffraction peak with different strip periodicities. One can see that the changes of the amplitude in the first diffraction peak with different strip periodicities can also be divided into four regions as those with $\lambda = 4l_{sp}$ Moreover, a narrower strip periodicity corresponds to an earlier phase inversion and an earlier appearance of the uniformly spaced droplet arrays in strips.

4. Conclusions

In this paper, the phase separation of polymer blend films on the stripe patterned surface is numerically investigated. Compared to experimental measurements, the simulated results exhibit more complete kinetic pathways of pattern-directed phase separation. The kinetic pathway and its mechanisms are analyzed in both real space and reciprocal space. It is found that the extreme fluctuation of the chemical potential at the edges of stripes leads to the formation of the branch structure. The alternation of in-phase and out-of-phase is found along the surface effect direction, demonstrating the phase inversion occurs not only in the polymer/air interface but also in the bulk. Essentially, the phase inversion in PDPS system is due to the interplay between the surface potential and the bulk chemical potential. The analysis in reciprocal space indicates that the evolution of the phase morphologies in the polymer/air interface obeys a $^1/_3$ power law for a thick film, consistent with the experimental results of Nisato et al. Our simulated results demonstrate that the phase inversion can extensively affect the relations between the diffraction peaks in the spectrum of anisotropic component and the character scale of the phase separation. It can also be found that the amplitude change of the first diffraction peak can reflect the kinetic pathway of the phase structure in the polymer\air interface very well. A narrower strip periodicity corresponds to an earlier phase inversion and an earlier appearance of the uniformly spaced droplet arrays in strips.

Acknowledgment. Financial supports from the National Natural Science Foundation of China (No. 90103035, No. 20174022, and No. 10334020) are highly appreciated. L.-T.Y acknowledges the Alexander von Humboldt Foundation for the support.

References and Notes

(1) (a) Binder, K. *Adv. Polym. Sci.* **1989**, *138*, 1. (b) Puri, S. *J. Phys.: Condens. Matter* **2005**, *17*, R101.
(2) Jones, R. A. L.; Norton, L.; Kramer, E. J.; Bates, F. S.; Wiltzius, P. *Phys. Rev. Lett.* **1991**, *66*, 1326.
(3) Bruder, F.; Brenn, R. *Phys. Rev. Lett.* **1992**, *69*, 624.

(4) Steiner, U.; Klein, J.; Eiser, E.; Budkowski, A.; Fetter, L. J. *Science* **1992**, *258*, 1126.
(5) (a) Krausch, G.; Kramer, E. J.; Rafailovich, M. H.; Sokolov, J. *Appl. Phys. Lett.* **1994**, *64*, 2655. (b) Böltau, M.; Walheim, S.; Mlynek, J.; Krausch, G.; Steiner, U. *Nature* **1998**, *391*, 877.
(6) (a) Ermi, B. D.; Nisato, G.; Douglas, J. F.; Rogers, J. A.; Kramer, A. *Phys. Rev. Lett.* **1998**, *81*, 3900. (b) Nisato, G.; Ermi, B. D.; Douglas, J. F.; Kramer, A. *Macromolecules* **1999**, *32*, 2356.
(7) (a) Li, X.; Xing, R.; Zhang, Y.; Han, Y.; An, L. *Polymer* **2004**, *45*, 1637. (b) Zhou, S.; Chakrabarti, A. *Polymer* **2001**, *42*, 6141.
(8) Rockford, L.; Liu, Y.; Mansky, P.; Russell, T. P.; Yoon, M.; Mochrie, S. G. *Phys. Rev. Lett.* **1999**, *82*, 2602.
(9) (a) Raczkowska, J.; Cyganik, P.; Budkowski, A.; Bernasik, A.; Rysz, J.; Rapits, I.; Czuba, P.; Kowalski, K. *Macromolecules* **2005**, *38*, 8488. (b) Raczkowska, J.; Bernasik, A.; Budkowski, A.; Gao, B.; Lieberman, M. *Macromolecules* **2007**, *40*, 2120.
(10) Yoo, P. J.; Suh, K. Y.; Lee, H. H. *Macromolecules* **2002**, *35*, 3205.
(11) Fukunaga, K.; Elbs, H.; Krausch, G. *Langmuir* **2000**, *16*, 3474.
(12) (a) Karim, A.; Douglas, J. F.; Lee, B. P.; Glotzer, S. C.; Rogers, J. A.; Jackman, R. J.; Amis, E. J.; Whitesides, G. M. *Phys. Rev. E* **1998**, *57*, R6273. (b) Johnson, W. C.; Wise, S. M. *Appl. Phys. Lett.* **2002**, *81*, 919. (c) Li, X.; Denn, M. M. *Ind. Eng. Chem. Res.* **2004**, *43*, 354.
(13) Kielhorn, L.; Muthukumar, M. J. *Chem. Phys.* **1999**, *111*, 2259.
(14) (a) Cahn, J. W.; Hilliard, J. E. J. *Chem. Phys.* **1958**, *28*, 258. (b) Cahn, J. W. J. *Chem. Phys.* **1965**, *42*, 93. (c) Cook, H. E. *Acta. Metall.* **1970**, *18*, 297.
(15) (a) Flory, P. J. *Principles of Polymer Chemistry*; Cornell University Press: Ithaca, NY, 1953. (b) de Gennes, P. G. *J. Chem. Phys.* **1980**, *72*, 4756.
(16) (a) Puri, S.; Binder, K. *Phys. Rev. A* **1992**, *46*, R4487. (b) Puri, S.; Binder, K. *Phys. Rev. E* **1994**, *49*, 5359. (c) Puri, S.; Binder, K. *Phys. Rev. E* **1997**, *56*, 6991.
(17) (a) Henderson, I. C.; Clarke, N. *Macromolecules* **2004**, *37*, 1952. (b) Henderson, I. C.; Clarke, N. *Macromol. Theor. Simul.* **2005**, *14*, 435.
(18) Glotzer, S. C. *Annu. Rev. Comput. Phys.* **1995**, *2*, 1.
(19) (a) Oono, Y.; Puri, S. *Phys. Rev. A* **1988**, *38*, 434. (b) Puri, S.; Oono, Y. *Phys. Rev. A* **1988**, *38*, 1542.
(20) Ohta, T.; Enomoto, Y.; Harden, J. L.; Doi, M. *Macromolecules* **1993**, *26*, 4928.
(21) Chen, H.; Chakrabarti, A. J. *Chem. Phys.* **1998**, *108*, 6897.
(22) Furukawa, H. *Adv. Phys.* **1985**, *37*, 703.
(23) (a) Sung, L.; Karim, A.; Douglas, J. F.; Han, C. C. *Phys. Rev. Lett.* **1996**, *76*, 4368. (b) Wang, W.; Shiwaku, T.; Hashimoto, T. *Macromolecules* **2003**, *36*, 8088. (c) Yan, L.-T.; Xie, X. M. *Macromolecules* **2006**, *39*, 2388.
(24) (a) Liao, Y.; Su, Z.; Ye, X.; Li, Y.; You, J.; Shi, T.; An, L. *Macromolecules* **2005**, *38*, 211. (b) Geoghegan, M.; Ermer, H.; Jüngst, G.; Krausch, G. *Phys. Rev. E* **2000**, *62*, 940. (c) Yan, L.-T.; Xie, X. M. *J. Chem. Phys.* **2007**, *126*, 064908.

MA702616S